DETAILED-CONTOUR INSENSITIVE FEATURES FOR AUTOMATED ANALYSIS OF BREAST MASSES IN MAMMOGRAMS

Alfonso Rojas and Asoke K. Nandi

The University of Liverpool
Department of Electrical Engineering and Electronics
Brownlow Hill, Liverpool, L69 3GJ, UK

ABSTRACT

Four new features for the analysis of breast masses are presented. These features were designed to be insensitive to the exact shape of the contour of the masses, so that an approximate contour, such as one extracted via an automated segmentation algorithm, can be employed in their computation. The features measure the degree of spiculation of a mass and the local fuzziness of the mass margins. The features were tested for characterization (discrimination between circumscribed and spiculated) and diagnosis (discrimination between benign and malignant) of breast masses, using 319 masses and three different classifiers. Approximately 90% and 76% of correct classification in characterization and diagnosis, respectively, were achieved.

Index Terms— Breast masses, Mammography, Pattern classification, Diagnosis, Feature extraction.

1. INTRODUCTION

Analysis of breast masses in mammograms has been performed via features obtained from the shape of the masses, texture features, edge sharpness, spiculation measures, etc. [1–8]. Characterization of the margins of masses is particularly relevant since spiculation (needle-like structures radiating from the mass) and ill-defined margins are usually associated with malignancy, while circumscribed (well defined) margins indicate a mass that is probably benign. Texture features have been extensively tested for characterization and diagnosis of masses, with varying results among studies [3, 5]. In general, these features alone have not produced results that are as good as those obtained with other features.

Shape features are, according to some studies [1, 2, 6, 9], among the most successful features for both characterization and diagnosis of breast masses. The shape of masses, however, is not always clearly defined. This poses a problem because shape features, are very sensitive to differences between shapes. Thus, the studies in the literature that employ shape features have almost always relied on a human expert to provide a manual segmentation of the masses from which reliable features can be obtained [1–3, 6].

Edge sharpness features, including acutance, contrast, and other gradient measures and variations of these, measure how crisp the transition between a mass and its surrounding background is. If the transition is abrupt (e.g. a circumscribed mass in a low density background), computing the acutance measure is straightforward. However, if the transition is fuzzy (e.g. a spiculated mass in high density background), the main difficulty resides in actually locating and defining the transition region, before one can start to measure its characteristics. Edge sharpness features, as shape features, have proven to be quite successful for classification of masses. However, like shape features, the edge sharpness features are sensitive to differences in the shape of masses. This is because these employ the intensity values of the image along the direction of the normal to the shape at every point on the boundary of a mass [3, 5]. A major drawback of these features, as these are currently defined, is that their computation is unfeasible for automated computer methods alone. Most of the studies that include these features have employed manually-drawn contours of the masses.

The consistency of the success that can be obtained with shape and edge sharpness measures may be overestimated by some of the results reported in the literature, where manually-drawn contours have been used to extract the features. It is doubtful that such levels of performance can be achieved by the same features without the manually-drawn mass contours. In this paper we propose four features designed to use as little information as possible from the contour of the masses, so that an approximate contour (such as one extracted via an automated segmentation algorithm) can be employed in their computation. The use of automated contours and robust features could improve the efficiency of mammographic screening programs without a decrease in performance.

2. IMAGE DATABASE

A set of images from the mini-MIAS [10] database and from the DDSM [11] database are used for validation of the results. The test set consists of 319 regions of interest (ROIs) with 167 circumscribed masses and 152 spiculated masses. The selection of cases included lesions with different degrees of subtlety and different sizes, from images with different breast-tissue densities, and lesions of benign and malignant diagnoses (155 benign, 164 malignant). The ROIs were all adjusted to be 256×256 pixels at 200 μm per pixel and 8 bpp (256 gray levels); no masses larger than 256×256 pixels were included in the set. Manual segmentations were produced based on the intensity and gradient magnitude of the mammograms and the annotations provided by the databases. These are regarded as ground truth (GT) of the boundary of the masses. An ellipse called the guiding ellipse was obtained (using a least-squares curve fitting procedure) for each of the GT boundaries. The set of guiding ellipses was then used as a set of approximate boundaries, as if these had been produced by a hypothetical automated segmentation algorithm. In this way, the evaluation of the features can be performed independently from the performance of a real automated-segmentation algorithm. The set of GTs of the boundaries was employed exclusively to obtain the set of guiding ellipses, and in no other procedure.

A. Rojas is sponsored by the National Council of Science and Technology of Mexico (CONACYT).

3. FEATURES

3.1. Radial to Tangential Signature Information

The first feature is a measure of similarity between three different edge signatures of a breast mass. One of the signatures, the omnidirectional edge signature, contains all of the edge content in the mammographic image. The other two signatures, the radial edge signature and the tangential edge signature, are designed to retain only the edge content that appears oriented in a certain direction. Using a similarity measure one can compare the edge signatures of a mass in a mammographic image. From such a comparison it is possible to obtain an indication of the characteristics of the mass in terms of the similarity measure. This is the rationale behind our first feature, which is formally described below.

Consider a log-Gabor function [12, 13] with a transfer function $\mathcal{G}$. A bank of oriented filters, $F_{n,k}$ is defined by:

$$\begin{aligned} \mathcal{G}(w) &= \exp(-(log(w/w_0)^2)/2(log(\sigma_w))), && (1)\\ G(\theta) &= exp(-(\theta-\theta_0)/2\sigma_\theta^2), && (2)\\ F_{n,k} &= \mathcal{G}(w_n)G(\theta_k), && (3) \end{aligned}$$

where w_0 is the centre frequency of the filters, σ_w is used to obtain constant-shape ratio filters, $G(\theta)$ is a Gaussian spreading function which acts as an angular envelope oriented in direction θ, σ_θ is the standard deviation of $G(\theta)$ in the angular direction. The subscripts n and k indicate a particular scale (n) and orientation (k) of a filter in the filter bank.

Let I be the 2-D DFT of a ROI containing a breast mass, with the mass centred on the ROI. Then the radial response $r_{n,k}$, the tangential response $t_{n,k}$, the radial edge signature $R(i,j)$, the tangential edge signature $T(i,j)$ and the omnidirectional edge signature $O(i,j)$ of the ROI are given by:

$$\begin{aligned} E_{n,k} &= \mathcal{F}^{-1}[IF_{n,k}], && (4)\\ r_{n,k} &= |E_{n,k}|G(\theta_k), && (5)\\ t_{n,k} &= |E_{n,k\perp}|G(\theta_k), && (6)\\ R(i,j) &= \sum_n \sum_k r_{n,k}(i,j), && (7)\\ T(i,j) &= \sum_n \sum_k t_{n,k}(i,j), && (8)\\ O(i,j) &= \max_{n,k} |E_{n,k}(i,j)|, && (9) \end{aligned}$$

where $E_{n,k}$ represents the complex response of one filter for a certain scale n and orientation k, and $k \perp$ is used to indicate the orientation orthogonal to orientation k. The spatial horizontal and vertical variables for the location of a pixel are represented by i and j, respectively.

Once the edge signatures have been computed, the spatial portions of the signatures that roughly correspond to the mass boundary are selected. The selection of the signature regions corresponds to a ribbon of 20 pixels centred on the guiding ellipse of each mass, which represents an estimate of the area where the boundary of each mass is located. This procedure is illustrated in Fig. 1.

Let $R_{\hat{B}}$, $T_{\hat{B}}$ and $O_{\hat{B}}$, represent the selected portions of the radial, tangential and omnidirectional signatures, respectively, and let $M(X;Y)$ represents the 2-D mutual information [14], between images X and Y.Then, the dimensionless feature Sp_{SI}, can be defined as:

$$Sp_{SI} = \frac{M(O_{\hat{B}}, R_{\hat{B}})}{M(O_{\hat{B}}, T_{\hat{B}})}. \quad (10)$$

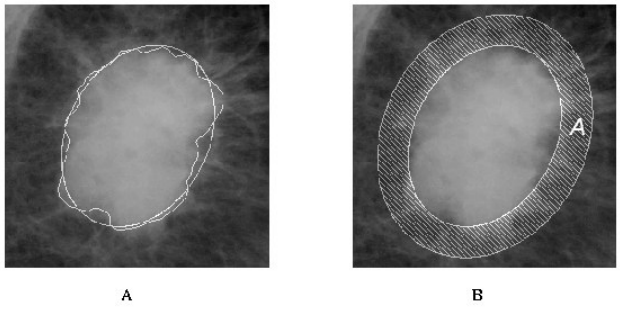

Fig. 1. A: Example of a spiculated mass, its GT, and guiding ellipse. B: The hatched region represents the locations to which the selection of pixels for computation of the Sp_{SI} and Sp_{GO} is restricted. The region is a ribbon of pixels around the guiding ellipse in A.

The larger the value of Sp_{SI} for a given mammographic mass, the most likely it is that the mass is a spiculated mass.

3.2. Relative Gradient Orientation

Our second feature is a spiculation measure based on the relative gradient orientation of pixels on spiculations, Sp_{GO}. Spiculations appear as linear structures with a positive image contrast. As a result of this, the gradient directions at image pixels on or close to the spicules have approximately the same orientation relative to the spicules. Spicules develop in an approximately radial direction to the mass, and the gradient at the pixels on a spicule is orthogonal to the direction of the spicule (Fig. 2-A). The Sp_{GO} feature exploits this relationship between the image gradient direction and the spicules direction to discriminate between spiculated and non-spiculated masses. In the ideal case of a perfectly circular mass, the angle θ between the gradient g and the line $\overline{PP'}$ is the same as the angle between g and the line $\overline{CP'}$, and this angle is approx. $\pi/2$ (Fig. 2-A). In a real case the mass is not circular. Thus the angle θ between g and $\overline{PP'}$ is different than the angle β between g and $\overline{CP'}$ (Fig. 2-B). Our feature measures the angle β (an approximation of θ), with the advantage that the boundary point P is not needed to measure it.

Our Sp_{GO} feature is defined as the average value of the sine function of the angle β, computed over a selection of pixels around the mass. In order to select the pixels we employ a feature known as the Phase Congruence (PC) [15]. The PC is a dimensionless measure of edge content with a range of [0-1]. Thus, it is possible to use a threshold on the PC image to pick up increasingly (or decreasingly) significant image features. A second restriction is imposed on the location of the pixels selected. The location was limited to a ribbon of 30 pixels around the guiding ellipse of each mass (Fig.1).

Let $\hat{g}_i$ represent the unitary gradient vector at a pixel location P'_i, and $\hat{c}_i$ represent the unitary vector with the direction of the line $\overline{CP'_i}$ joining the centroid of the mass, C, and the selected pixel P'_i. Then, the Sp_{GO} is mathematically expressed as:

$$\begin{aligned} Sp_{GO} &= \frac{1}{N}\sum_i \sin(\arccos(\hat{g}_i \cdot \hat{c}_i)), && (11)\\ i &\in \{A \cap (PC(x,y) > \alpha)\}, \qquad i = 1, 2, \ldots, N. \end{aligned}$$

where N is the total number of selected pixels, A represents the selection-allowed region (see Fig. 1-B), $PC(x,y)$ is the phase congruence value of the pixel at location (x,y), and $\alpha \in (0-1)$ is a

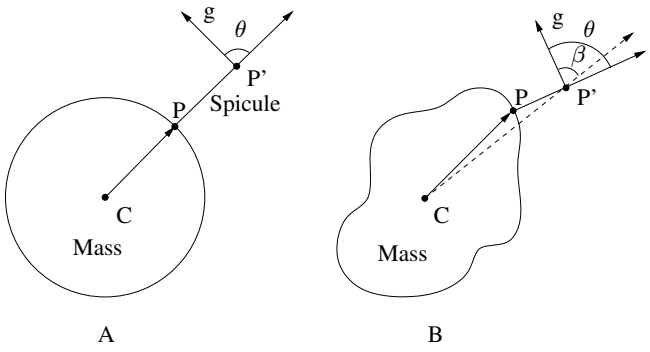

Fig. 2. The contour of the mass is represented by a circle, the line containing the segment $\overline{PP'}$ represents a spicule, and the vector g represents the gradient direction at point P' on the spicule. A: Ideal case of a perfectly circular mass. B: In a real case the mass is not circular, and the angle θ is different than the angle β

.

threshold on the phase congruence that becomes a parameter of the Sp_{GO} feature.

3.3. Measures of the fuzziness of mass margins

These two features are measures of the local fuzziness of the mass margins. The method to compute these is more easily implemented and described on the polar-variable representation of the ROIs. In this representation, $(x, y) \mapsto (r, \theta)$, with the centroid of the mass as the origin of the transformation, $r = 1, 2, \ldots, 128$ (maximum valid radius in ROIs of size 256×256), and $\theta = 1, 2, \ldots, 360$. Let (i, j) represent the indexes in the polar representation of the ROIs.

First we compute the derivative (first or second order) in the radial direction. Next, we find the pair of points, separated a fixed distance apart along the radial direction, δ_i, for which the difference between derivative values is maximum. This is done along the angular variable. The location halfway between these points is the location of the strongest edge in the radial direction, which we use to characterize the mass margins. The location of the strongest-edge is restricted to a band of pixels around the guiding ellipse to reduce possible noise being included. By computing the average of the radial difference between strongest-edge locations along the tangential direction, we obtain an indicator or measure of the fuzziness of the mass margins. This is mathematically expressed as:

$$d_k(i,j) = |p_k(i-\delta_i, j) - p_k(i+\delta_i, j)|, \quad (12)$$

$$m_k(j) = \arg\max_i d_k(i,j), \quad (13)$$

$$Fz_k = \frac{1}{J}\sum_j |m_k(j) - m_k(j+1)| \quad (14)$$

where $p_k(i, j)$ represents the k-th order difference in the radial direction, $k = \{1, 2\}$, and J represents the maximum of index j. It should be noted that in the definition of the features Fz_1 and Fz_2 (Fz stands for *fuzziness* of the mass margin), the radial direction is being employed as a rough approximation to the direction which is normal to the mass contour (which we assume is unknown). Thus, the shape of the masses are implicitly assumed to be circular.

4. EXPERIMENTAL RESULTS

The characterization (circumscribed vs. spiculated classification) and diagnosis (benign vs malignant classification) abilities of the features presented in Section 3 were tested using three binary classifiers. The Fisher's Linear Discriminant (FLD), a Bayesian classifier (BCLS), and a support vector machine (SVM). Our whole set of 319 masses was employed in this test under a leave-one-out classification framework. None of the parameters of the classifiers were optimised for our particular dataset. The features were tested individually and in combination. The main results of the experiments are reported in Table 1. In the case of Sp_{GO}, the number reported is the performance with $\alpha = 0.5$, which is a value in the middle of the range of this parameter (in experiments not reported here due to space limitations, it was found that Sp_{GO} is not very sensitive to the value of α when this parameter is in the middle range).

Table 1. Performance - Characterization and Diagnosis.

Features or feature-sets	Charact. (%)		Diagnosis (%)	
	Avg.	Std. Dev.	Avg.	Std. Dev.
Fz_2 & Sp_{SI}	89.8	0.7	76.1	0.3
All features	89.6	1.0	75.9	0.3
Fz_2 & Sp_{SI} & Sp_{GO}	89.4	1.0	76.0	0.6
Fz_1 & Fz_2 & Sp_{SI}	89.1	0.8	75.8	0.5
Fz_1 & Sp_{SI} & Sp_{GO}	88.5	0.8	73.4	0.6
Fz_1 & Sp_{SI}	87.7	0.5	73.5	0.6
Sp_{SI}	87.6	0.4	73.2	0.4
Sp_{SI} & Sp_{GO}	87.3	0.2	73.1	0.3
Fz_2 & Sp_{GO}	86.3	0.2	73.1	0.3
Fz_1 & Sp_{GO}	85.1	0.4	72.1	0.0
Fz_1 & Fz_2 & Sp_{GO}	84.8	0.5	72.8	0.3
Sp_{GO}	79.6	0.8	66.5	0.6
Fz_1	75.3	0.2	67.2	1.0
Fz_1 & Fz_2	75.0	0.7	66.8	1.2
Fz_2	71.7	0.2	67.0	0.3

In order to test the robustness of our features to variations of the boundary used as a guide in their computation, the classification experiments described above were performed several times, each time using a set of guiding ellipses slightly modified from the original set.

The original set of ellipses were rotated fifteen degrees clockwise at a time, producing a super-set of ellipses rotated 0, 15, 30, 45, 60 and 90 degrees with respect to their original orientation. As the ellipses are rotated in increasing amounts, the area overlap measure (AOM, a measure of the agreement between two image regions) between the rotated and the original ellipses decreases. In this way we simulated the effect of segmentations with varying degrees of agreement to the actual shape of the masses. The main results of this test are reported in Table 2, where the first column contains the average AOM between the original and rotated ellipses, computed over the whole test dataset. The corresponding amount of rotation from the original orientation is also given.

5. DISCUSSION AND CONCLUSIONS

Considering the average (over the three classifiers) characterization performance of each single feature and ordering the features from most to least efficient, we have: 1.- Sp_{SI}, 2.- Sp_{GO}, 3.- Fz_1, and 4.- Fz_2. This result is not surprising, since we know that the Fz_k features contain more approximations than Sp_{GO}, which in turn also

Table 2. Robustness test - Characterization and Diagnosis.

Avg. AOM (rotation)		Charact. (%)			Diagnosis (%)		
		Fz_1	Fz_2	Sp_{GO}	Fz_1	Fz_2	Sp_{GO}
0.89	(0°)	75.3	71.7	79.6	67.2	67.0	66.5
0.86	(15°)	74.9	71.1	79.6	67.8	66.2	67.8
0.80	(30°)	71.4	71.2	79.0	66.7	65.5	65.7
0.76	(45°)	71.1	71.3	77.7	65.8	65.6	65.3
0.72	(60°)	72.8	68.8	79.6	67.8	65.5	66.0
0.70	(75°)	69.6	66.2	79.4	66.0	64.5	65.7
0.69	(90°)	70.5	67.0	78.1	64.9	63.4	65.9
Average		72.2	69.6	79.0	66.6	65.5	66.1
Std. Dev.		2.2	2.3	0.8	1.1	1.2	0.8

contains more approximations than Sp_{SI}. Considering now the average performance obtained by combinations of features, we observe that the difference between the top results is not statistically significant. The overall highest performance was obtained with the SVM classifier and the set of all features, reaching 90.6 % characterization success.

The robustness test shows that for a reduction of 20% of the average AOM between the set of guiding ellipses and the set of GT regions, the average range of variation of the characterization performance is 4.3%, while the average range of variation of the diagnosis performance is only 3%. The average standard deviation over all the features is 1.4%. For the range of AOM considered, the classification performance is quite stable and its decrease is about five times smaller than the decrease of the segmentation quality. This results demonstrate that the performances from the features are effectively robust to changes of the boundary of masses. Furthermore, it should be obvious that it would be useless attempting to classify the masses in the dataset using shape measures obtained from the set of guiding ellipses. Other popular features, such as edge sharpness measures could also be affected by the missing boundary information. In contrast, the features presented in this paper achieve good classification performance using the set of ellipses. In other words, our features are, to some degree, insensitive to the accuracy of the mass boundaries, which is an advantage if the features are to be employed in automated feature-extraction.

The classification results obtained by our features, in combination with commonly used classifiers employed in an off-the-shelf fashion, demonstrate that effective characterization of breast masses is possible without employing any of the commonly used shape features. The performance achieved by our features in the characterization experiments (approx. 90% success) is comparable to some of the best results reported in the literature [1, 2, 4–6, 16]. Using our features in combination with complementary features (i.e. measures of other useful characteristics) as well as more sophisticated and tuned classifiers can be expected to improve the classification performance.

6. REFERENCES

[1] R. M. Rangayyan, N. M. El-Faramawy, J. E. L. Desautels, and O. A. Alim, "Measures of acutance and shape for classification of breast tumors," *IEEE Trans. Med. Imag.*, vol. 16, no. 6, pp. 799–810, December 1997.

[2] R. M. Rangayyan, N. R. Mudigonda, and J. E. L. Desautels, "Boundary modelling and shape analysis methods for classification of mammographic masses," *Medical & Biological Engineering & Computing*, vol. 38, no. 5, pp. 487–496, September 2000.

[3] T. C. S. S. André and R. M. Rangayyan, "Classification of breast masses in mammograms using neural networks with shape, edge-sharpness, and texture features," *Journal of Electronic Imaging*, vol. 15, no. 1, pp. 013019–1–10, Jan-Mar 2006.

[4] B. Sahiner, H.-P Chan, N. Petrick, M. A. Helvie, and L. M. Hadjiiski, "Improvement of mammographic mass characterization using spiculation measures and morphological features," *Med. Phys.*, vol. 28, no. 7, pp. 1455–1465, July 2001.

[5] C. Varela, S. Timp, and N. Karssemeijer, "Use of border information in the classification of mammographic masses," *Physics in Medicine and Biology*, vol. 51, no. 2, pp. 425–441, January 2006.

[6] R. M. Rangayyan and T. M. Nguyen, "Fractal analysis of contours of breast masses in mammograms," *Journal of Digital Imaging*, October 2006, Doi: 10.1007/s10278-006-0860-9.

[7] P. Delogu, M. E. Fantacci, P. Kasae, and A. Retico, "Characterization of mammographic masses using a gradient-based segmentation algorithm and a neural classifier," *Computers in Biology and Medicine*, 2007, Doi: 10.1016/j.compbiomed.2007.01.009.

[8] J-L Viton, M. Rasigni, G. Rasigni, and A. Llebaria, "Method for characterizing masses in digital mammograms," *Optical Engineering*, vol. 35, no. 12, pp. 3453–3459, December 1996.

[9] R. J. Nandi, A. K. Nandi, R. M. Rangayyan, and D. Scutt, "Classification of breast masses in mammograms using genetic programming and feature selection," *Medical and Biological Engineering and Computing*, vol. 44, no. 8, pp. 683–694, August 2006.

[10] J. Suckling, J. Parker, D. Dance, S. Astley, I. Hutt, C. Boggis, I. Ricketts, E. Stamatakis, N. Cerneaz, S. Kok, P. Taylor, D. Betal, and J. Savage, "The Mammographic Image Analysis Society digital mammogram database," *Exerpta Medica, International Congress Series 1069*, pp. 375–378, 1994.

[11] M. Heath, K. W. Bowyer, and D. Kopans et. al, "Current status of the digital database for screening mammography," in *Digital Mammograpy*, N. Karssemeijer, M. Thijssen, J. Hendriks, and L. van Erning, Eds., pp. 457–460. Kluwer Academic Publishers, Boston, Massachusetts, USA, 1998.

[12] P. Kovesi, "Phase congruency detects corners and edges," *In proceedings of The Australian Pattern Recognition Society Conference: DICTA 2003. Sydney.*, pp. 309–318, December 2003.

[13] Z. Wang and M. Jenkin, "Using complex gabor filters to detect and localize edges and bars," in *Advances in machine vision: strategies and applications*, C. Archibald and E. Petriu, Eds., pp. 151–170. World Scientific Publishing Co., Inc. River Edge, NJ, USA, 1992.

[14] T. M. Cover and J. A. Thomas, *Elements of Information Theory*, Wiley-Interscience, New Jersey, USA, 2 edition, 2006.

[15] P. Kovesi, "Image features from phase congruency," *Videre: Journal of Computer Vision Research, The MIT Press*, vol. 1, no. 3, pp. 1–26, 1999.

[16] M. P. Sampat, M. K. Markey, and A. C. Bovik, "Computer-aided detection and diagnosis in mammography," in *Handbook of Image and Video Processing*, A. C. Bovik, Ed., pp. 1195–1217. Elsevier Academic Press, 2 edition, 2005.